Materials Science and Engineering B 327 (2026) 119266

Contents lists available at ScienceDirect

Materials Science & Engineering B

journal homepage: www.elsevier.com/locate/mseb

Interfacial modulation in OPVA–ZnO–GO nanocomposites for enhanced proton transport and emission control

Ridha Elleuch [a], Khaled Charradi [b,c], Abdullah Y.A. Alzahrani [d], Soad Z. Alsheheri [e], Akram Alhussein [f], Youssef O. Al-Ghamdi [g], Sherif M.A.S. Keshk [c,*]

[a] Institut des Molécules et Matériaux du Mans (IMMM-UMR CNRS 6283), Université du Mans, Avenue Olivier Messiaen, 72085 Le Mans, CEDEX 9, France
[b] Nanomaterials and Systems for Renewable Energy Laboratory, Research and Technology Center of Energy, Technopark Borj Cedria, BP 095 Hammam Lif, Tunisia
[c] BECOME:Deep Tech & Nanoscience, 63 Rue De Tolbiac, 75013, Paris, France
[d] Department of Chemistry, Faculty of Science, King Khalid University, Abha 61413, Saudi Arabia
[e] Chemistry Department, Faculty of Science, King Abdulaziz University, P.O. Box 80203, Jeddah 21589, Saudi Arabia
[f] LASMIS research unit, University of Technology of Troyes, Technological Pole of South Champagne, Lavoisier Rd, 52800 Nogent, France
[g] Department of Chemistry, College of Science Al-zulfi, Majmaah University, Al-Majmaah 11952, Saudi Arabia

ARTICLE INFO

Keywords:
Oxidized polyvinyl alcohol (OPVA)
In situ ZnO synthesis
Graphene oxide (GO), co-doping
Mechanical response
Proton conductivity
Optical transparency

ABSTRACT

Flexible electronic platforms require polymer nanocomposites that integrate high optical transparency, tunable photoluminescence (PL), and efficient proton transport. Conventional poly(vinyl alcohol) (PVA) systems often suffer from limited chain mobility and poor nanoparticle dispersion, leading to trade-offs among these properties. To address limitations in conventional PVA systems, namely poor nanoparticle dispersion, limited chain mobility, and suboptimal hydrogen bonding, we present a carbonyl-rich oxidized PVA (OPVA) matrix doped with ZnO nanoparticles and graphene oxide (GO). The nanocomposites were fabricated *via in situ* ZnO synthesis and GO-mediated interfacial modulation. GO facilitates defect passivation and proton hopping, while ZnO contributes to crystallite refinement and emission control. At 1 wt% GO loading, the composite exhibits a three-fold increase in photoluminescence intensity, suppression of defect-related bands, and a two-order magnitude enhancement in proton conductivity (1.2×10^{-3} S/cm). Optical transparency exceeds 85% in the visible range, and mechanical strength improves by over 35%. These findings validate OPVA–ZnO–GO nanocomposites as scalable, multifunctional materials for transparent electronics, ionic membranes, and optoelectronic wearables.

1. Introduction

Polymer-based nanocomposites have emerged as versatile platforms for multifunctional materials, particularly in optoelectronics, energy conversion, and membrane technologies. Among these, oxidized polyvinyl alcohol (OPVA) matrices doped with zinc oxide (ZnO) nanoparticles have demonstrated promising enhancements in optical transparency, mechanical strength, and proton conductivity, especially when synthesized *via in situ* protocols that promote nanoparticle dispersion and strong interfacial bonding [1–4]. The semiconducting nature of ZnO, combined with its high exciton binding energy and UV-blocking capability, makes it a highly attractive filler for polymer matrices [5–7]. Despite these advantages, ZnO/OPVA systems often encounter limitations at higher ZnO loadings, where nanoparticle aggregation compromises flexibility, conductivity, and optical clarity [8–10]. To overcome these challenges, recent studies have explored the incorporation of graphene oxide (GO) into ZnO–polymer systems, leveraging GO's high aspect ratio, rich surface chemistry, and defect-passivation properties [10–12]. The oxygen-containing functional groups of GO (–OH, –COOH, epoxy) enable strong hydrogen bonding and electrostatic interactions with both OPVA and ZnO, potentially stabilizing dispersion, enhancing charge transport, and reinforcing mechanical integrity [13–15]. In ZnO–GO hybrids, GO has been shown to suppress electron–hole recombination, improve photoluminescence (PL) purity, and facilitate proton hopping through extended hydrogen-bonded networks [16,17]. Building on these insights, this study introduces a ternary OPVA–ZnO–GO nanocomposite system, where GO is incrementally incorporated (0.5–1.5 wt%) into a preformed OPVA–ZnO matrix. The central hypothesis is that GO acts not merely as a passive filler but also as an active interfacial modulator, enhancing ZnO

* Corresponding author.
E-mail address: sherif.keshk@become.institute (S.M.A.S. Keshk).

https://doi.org/10.1016/j.mseb.2026.119266
Received 22 November 2025; Received in revised form 16 January 2026; Accepted 31 January 2026
Available online 4 February 2026

dispersion, tuning optical and proton-conductive properties, and reinforcing the polymer network. This approach is supported by recent findings in ZnO/GO systems, where the lamellar structure and π-conjugated domains of GO have been shown to facilitate defect engineering and broadband optical modulation [7,18]. The novelty of this work lies in its strategic co-engineering of ZnO and GO within a carbonyl-rich OPVA matrix using a scalable, solution-processable route. In contrast to ZnO/OPVA systems, this ternary design enables the simultaneous optimization of transparency, conductivity, and mechanical resilience, key attributes for flexible electronics, UV-shielding films, and proton exchange membranes [19,20]. The rationale for selecting GO is multifaceted. First, the π-conjugated domains and defect sites of GO facilitate electron and proton hopping, a property which is critical for optoelectronic and energy-related applications [21,22].

Second, GO has been shown to suppress electron-hole recombination in ZnO-based systems, thereby improving both PL and photocatalytic efficiency [23,24]. Third, the mechanical robustness and high Young's modulus of GO contribute to matrix reinforcement, particularly at low loadings, where it functions as a stress transfer agent without inducing brittleness [25,26]. Fourth, the inclusion of GO aligns with sustainable material design principles, as it is derived from graphite through oxidation, making it a scalable and environmentally benign additive [27,28]. OPVA provides a more reactive matrix than PVA, enabling stronger interactions with GO. Recent OPVA–GO studies show high transparency and improved proton transport at low GO loadings. Optical measurements also reveal tunable bandgaps and suppressed reflectance arising from GO-induced electronic coupling [29]. This study further builds on recent advances in defect engineering and energy transfer mechanisms. PL analysis under UV excitation was employed to probe ZnO defect states (*e.g.*, oxygen vacancies, zinc interstitials) and to assess the role of GO in modulating radiative recombination [30]. Time-resolved PL and temperature-dependent conductivity measurements are expected to further confirm the role of GO in enhancing charge mobility and suppressing non-radiative losses [3,31]. To validate the hypothesis, a comprehensive suite of characterization techniques, including Fourier transform infrared (FTIR) spectroscopy, X-ray diffraction (XRD), scanning electron microscopy (SEM), ultraviolet-visible (UV–Vis) spectroscopy, PL, electrochemical impedance spectroscopy (EIS), and tensile testing, is employed. The expected outcomes include: (i) improved ZnO dispersion and reduced aggregation at optimal GO loadings, (ii) enhanced bandgap tunability and UV-blocking efficiency, (iii) increased proton conductivity through GO-mediated transport channels, and (iv) balanced mechanical reinforcement without compromising flexibility. Collectively, these findings are intended to establish OPVA–ZnO–GO nanocomposites as a new class of multifunctional materials for next-generation energy and photonic platforms. From a materials design perspective, this system exemplifies that targeted chemical modification, specifically the oxidation of PVA, introduces new functionalities into polymer matrices. OPVA serves a dual role as both a reactive host and a flexible scaffold, enabling precise control over nanoparticle behavior and composite architecture. The *in situ* synthesis route ensures uniform dispersion and minimizes phase separation, while GO co-doping allows tunable property enhancement without compromising transparency or flexibility [32,33]. In summary, this study advances the rational design of multifunctional polymer nanocomposites by incorporating ZnO and GO into an OPVA matrix. The resulting composite functions as a flexible material for transparent electronics, sensing membranes, and proton-conductive surfaces, effectively integrating optical transparency, ionic transport, and mechanical durability. It is proposed that GO-mediated interfacial polarization and ZnO-driven crystallite refinement work together to increase photoluminescence intensity, proton conductivity, and tensile strength. All of these concepts are effectively elucidated through structural, optical, and electrochemical analyses, leading to an approach for next-generation electronic materials.

2. Experimental

2.1. Materials and reagents

Polyvinyl alcohol (PVA) with a molecular weight in the range of 89,000–98,000 and a hydrolysis degree exceeding 99% was sourced from Sigma-Aldrich and utilized as received without further purification. Sodium periodate ($NaIO_4$), graphite powder, concentrated sulfuric acid (H_2SO_4), and potassium permanganate ($KMnO_4$), all required for the synthesis of GO, were obtained from Fluka. All aqueous solutions were prepared using ultrapure deionized water (resistivity $\geq$18.2 MΩ·cm) obtained from a Millipore purification system.

2.2. Preparation of oxidized polyvinyl alcohol (OPVA)

OPVA was synthesized through the selective oxidation of PVA using $NaIO_4$ under controlled conditions [34]. A 10 wt% PVA solution was reacted with 0.5 M equivalents of $NaIO_4$ at 40 °C for 2 h in the dark to prevent side reactions. The oxidized product was purified *via* dialysis (molecular weight cutoff: 12–14 kDa) for 48 h, followed by freeze-drying. The resulting OPVA retained its film-forming capability and exhibited carbonyl functionalities suitable for subsequent composite integration.

2.3. Synthesis of graphene oxide (GO)

GO was produced using a modified Hummers' protocol [29,35]. Graphite powder was oxidized in concentrated H_2SO_4 with $KMnO_4$, under temperature-controlled conditions. The reaction was quenched by the addition of H_2O_2, and the resulting suspension was subjected to repeated centrifugation and washing with hydrochloric acid and deionized water. The purified GO was then sonicated for 1 h to achieve exfoliation into nanosheets. The final dispersion was prepared at a concentration of 2 mg/mL for use in composite fabrication.

2.4. Preparation of zinc oxide precursor solution

Zinc oxide was generated *via* the alkaline hydrolysis of zinc acetate dihydrate ($Zn(CH_3COO)_2{\cdot}2H_2O$) [4]. The salt was dissolved in deionized water under ambient conditions, and the pH of the solution was carefully adjusted to 10 using a 1 M sodium hydroxide solution.

The mixture was stirred for 30 min to initiate ZnO nanoparticle formation. This procedure was repeated with varying concentrations of zinc acetate to modulate the ZnO content in the resulting composite system.

2.5. In situ formation of ZnO within OPVA matrix

Instead of synthesizing ZnO separately and blending it post-synthesis, this study employed an *in situ* approach to embed ZnO nanoparticles directly within the OPVA matrix. OPVA was first obtained by oxidizing PVA using $KMnO_4$, yielding a carbonyl-functionalized polymer in powder form. To incorporate ZnO, a pre-prepared zinc acetate solution (pH 10) was added to the OPVA dispersion and stirred continuously at 80 °C. This thermal treatment promoted uniform nucleation and growth of ZnO nanoparticles within the polymer network, enhancing interfacial bonding and reducing aggregation. The resulting ZnO–OPVA mixture was cast into Petri dishes and dried at 90 °C to form flexible membranes. Samples were prepared with ZnO loadings of 1 wt%, 5 wt%, and 10 wt% to investigate concentration-dependent effects on structural, optical, and conductive properties.

2.6. Fabrication of OPVA ZnO–GO composite membranes

Composite films were prepared using a solution-casting method. OPVA (5 wt%) was dissolved in deionized water at 60 °C under

continuous stirring. GO was introduced at concentrations of 0.5 wt%, 1.0 wt%, and 1.5 wt% relative to the OPVA content. The mixtures were sonicated for 30 min to ensure uniform dispersion of GO within the polymer matrix. The resulting solutions were poured into Petri dishes and allowed to dry under ambient conditions for 48 h. The dried membranes were carefully peeled off, stored under vacuum, and thermally conditioned at 60 °C prior to characterization. Film thickness ranged from 80 to 120 μm.

2.7. Characterization techniques

FTIR spectra were acquired using a Bruker Alpha ATR spectrometer across the 4000–500 cm^{-1} range with a resolution of 4 cm^{-1}, averaging 32 scans per sample. Samples were pressed directly onto a ZnSe ATR crystal for analysis. Raman spectroscopy was performed at room temperature with a Jobin Yvon technology T6400 system, employing a 488 nm argon laser as the excitation source. The crystalline structure was examined using a PANalytical Empyrean diffractometer with Cu Kα radiation (λ = 1.5418 Å). Scans were conducted over a 2θ range of 5°–50° with a step size of 0.026° and a dwell time of 0.5 s per step. Crystallite sizes were estimated from the (101) reflection using the Scherrer equation, assuming a shape factor of 0.9.

The SEM images were obtained on a JEOL JSM 6510 LV microscope operating at an accelerating voltage of 15 kV.

Reflectance and transmittance measurements were performed using a Bruker Tenor27 spectrometer over the 300–1000 nm wavelength range with 1 nm resolution to validate optical uniformity across the samples. The room temperature PL spectra were recorded using a Shimadzu RF-6000 spectrofluorophotometer equipped with a 150 W Xenon lamp (Duisburg, Germany) under 266 nm and 900 nm excitation wavelengths. Furthermore, the mechanical properties of the membranes were studied using a universal testing machine (Instron USA, model 3365). Measurements included tensile strength (MPa), modulus (MPa), stiffness (KN/m), and elongation (%). Membrane thickness was measured at three different locations for each sample, with an average value of approximately 110 ± 10 μm. All measurement tests were conducted according to the ASTM D-882 standard (ASTM, 1992) at a testing speed of 10 mm/min. The wettability of the membranes was investigated using a contact angle test with an optical goniometer (Data Physics, Model ESr—N, Germany). Water droplet contact angles on the membrane surfaces were measured by dropping 5 μL of water at a rate of 2 μL/s.

3. Results and discussion

To elucidate the multifunctional enhancements imparted by GO co-doping in OPVA–ZnO nanocomposites, a comprehensive set of characterization techniques was employed. These analyses were designed to correlate structural, optical, mechanical, and proton-conductive properties with varying GO loading levels (0.5 wt%, 1 wt%, and 1.5 wt%). The results reveal a synergistic interplay among the carbonyl-rich OPVA matrix, the semiconducting ZnO nanostructure, and the interfacial versatility of GO. The following sections provide detailed insights into the GO's role in modulating interfacial bonding, nanoparticle dispersion, defect passivation, and charge transport, ultimately validating the hypothesis that low-level GO incorporation yields tunable and scalable performance across multiple functional domains.

3.1. FTIR spectroscopy

The FTIR spectra of OPVA–ZnO nanocomposites co-doped with varying GO ratios (0.5 wt%, 1 wt%, and 1.5 wt%) indicate a progressive transformation in the molecular architecture of the polymer matrix, driven by synergistic interactions among OPVA chains, ZnO nanoparticles, and GO nanosheets (Fig. 1).

In the spectrum of pristine OPVA (Fig. 1a), the broad O—H stretching band centered around 3400–3500 cm^{-1} reflects extensive hydrogen bonding among hydroxyl groups within the OPVA matrix. The distinct C═O stretching vibration near 1720 cm^{-1} confirms the successful oxidative modification of PVA, introducing carbonyl functionalities that increase polarity and coordination potential [1,2]. This modification alters the hydrogen bonding network and chain packing, creating a chemically active matrix capable of hosting inorganic nanoparticles and promoting interfacial interactions. Upon doping with 1 wt% ZnO (Fig. 1b), a new absorption band emerges near 500–550 cm^{-1}, belonging to Zn—O stretching vibrations, thereby confirming the *in situ* formation and integration of ZnO nanoparticles within the OPVA matrix [4]. Simultaneously, the O—H band intensity decreases, indicating partial disruption of the hydrogen bonding network due to ZnO coordination with the oxygenated groups of OPVA, particularly hydroxyl and carbonyl moieties [4,14]. This coordination reflects a shift from intra-polymer hydrogen bonding to polymer–nanoparticle interactions, enhancing structural rigidity and facilitating transport pathways. With the introduction of 0.5 wt% GO (Fig. 1c), the O—H band broadens and shifts slightly, suggesting the formation of new hydrogen bonding interactions between GO's hydroxyl and carboxyl groups and the OPVA matrix. The C═O band intensifies, likely due to overlapping contributions from GO's carboxylic functionalities, while a shoulder near 1620 cm^{-1} appears, corresponding to C═C skeletal vibrations of GO's sp^2-hybridized graphitic domains [10].

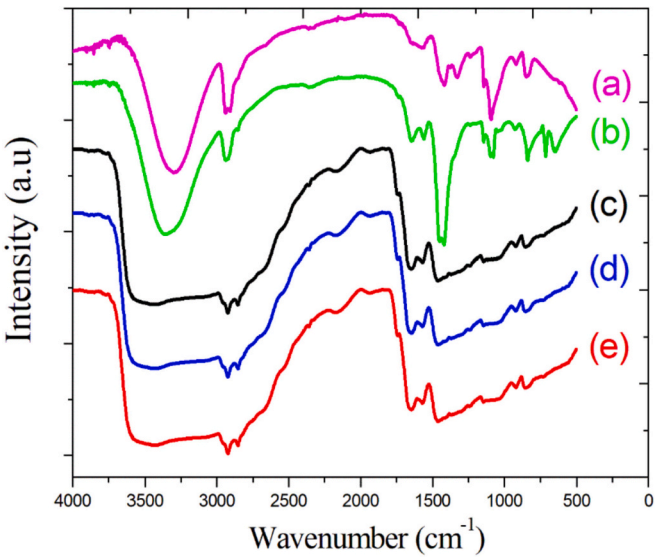

Fig. 1. FTIR spectra of **(a)** OPVA, **(b)** OPVA-ZnO, **(c)** OPVA-ZnO-GO (0.5 wt%), **(d)** OPVA-ZnO-GO (1 wt%), and **(e)** OPVA-ZnO-GO (1.5 wt%) membranes.

These spectral changes indicate the onset of ternary network formation, where GO modulates both chemical bonding and vibrational dynamics. At 1 wt% GO (Fig. 1d), these effects become more pronounced. The O—H and C═O bands exhibit further broadening and increased intensity, reflecting enhanced hydrogen bonding and dipolar interactions. A new band emerges near 1230 cm^{-1}, assigned to C–O–C stretching vibrations from GO's epoxy groups, confirming its chemical integration into the matrix [36]. Concurrently, the Zn—O band sharpens, implying improved nanoparticle dispersion and stronger interfacial coordination, likely facilitated by GO acting as a stabilizing scaffold and defect passivator. This spectral profile reflects optimal interfacial synergy, with GO promoting both chemical connectivity and nanoparticle alignment. At higher GO loading (1.5 wt%, Fig. 1e), the O—H band becomes broader but less intense, suggesting saturation of hydrogen-bonding sites and possible steric hindrance from excess GO. The C═O and C═C bands become more pronounced, highlighting GO's dominant spectral influence and partial phase segregation. The Zn—O band exhibits a slight decrease, likely due to nanoparticle shielding or

aggregation, which reduces ZnO accessibility and coordination efficiency [13]. These spectral shifts indicate that excessive GO disrupts the balance of the ternary network, compromising interfacial uniformity and vibrational coherence. Mechanistically, the FTIR evolution confirms the formation of a chemically integrated ternary system, with GO actively influencing hydrogen bonding, nanoparticle dispersion, and vibrational coupling. The optimal spectral synergy occurs at 1 wt% GO, where hydrogen bonding, ZnO coordination, and functional group definition are maximized. These observations support the hypothesis that GO acts not as a passive filler but as a dynamic interfacial modulator, enabling the tuning of optoelectronic and proton-conductive properties through controlled molecular engineering.

3.2. X-ray diffraction (XRD)

The XRD patterns of OPVA–ZnO nanocomposites co-doped with different GO ratios (0.5 wt%, 1 wt%, and 1.5 wt%) reveal progressive structural modulation and phase evolution, indicating the dynamic crystallization behavior and dispersion efficiency of ZnO nanoparticles within the oxidized polymer matrix (Fig. 2). In the pristine OPVA membrane (Fig. 2a), a broad amorphous halo centered at $2\theta \approx 19.5^{\circ}$ reflects the semi-crystalline nature of OPVA, attributed to disrupted hydrogen bonding and increased chain packing induced by oxidation [1,2]. This feature corresponds to the (101) plane of OPVA and yields a relatively large d-spacing of 4.55 Å, indicative of loose interchain packing and limited long-range order.

The calculated crystallite size of 3.3 nm, along with a crystallinity index (CI) of 0.42, confirms the matrix's amorphous character and its suitability for nanoparticle incorporation. Upon doping with 1 wt% ZnO (Fig. 2b), sharp diffraction peaks emerge at $2\theta \approx 31.7^{\circ}$, 34.4°, 36.2°, and 47.5°, corresponding to the (100), (002), (101), and (102) planes of hexagonal wurtzite ZnO (JCPDS 36–1451). These reflections confirm the successful *in situ* formation of ZnO crystallites within the OPVA matrix. However, XRD alone cannot provide direct evidence of homogeneous nanoparticle distribution; any inference of improved dispersion is based only on indirect indicators such as peak sharpening and reduced microstrain. True spatial uniformity must be verified using complementary techniques such as SEM [4]. Notably, the (101) peak at 36.2° becomes the dominant reflection, with a reduced d-spacing of 2.48 Å and an increased crystallite size of 12.4 nm. The CI increases to 0.72, indicating a substantial enhancement in structural ordering and nanoparticle alignment compared to pristine OPVA. With the addition of 0.5 wt% GO (Fig. 2c), the ZnO peaks remain discernible, although the (101) reflection exhibits slight broadening and reduced intensity. This behavior suggests mild lattice distortion and enhanced interfacial coupling between ZnO and GO nanosheets. The crystallite size increases to 14.9 nm, and the CI rises to 0.76, highlighting GO's role in promoting ZnO nucleation and dispersion.

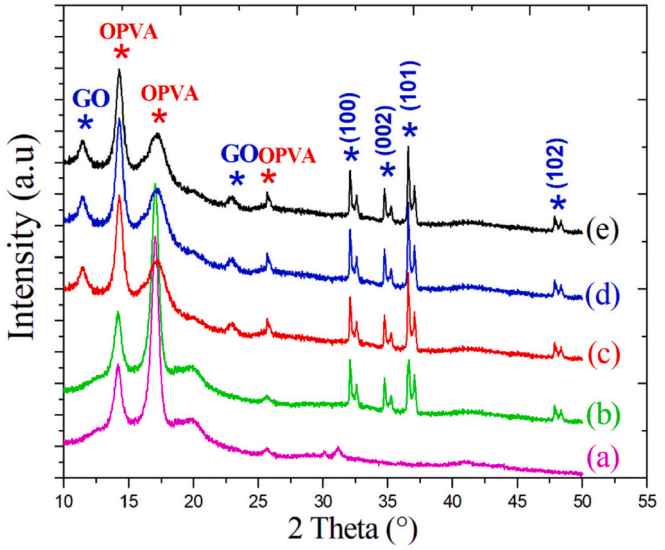

Fig. 2. XRD patterns of **(a)** OPVA, **(b)** OPVA-ZnO, **(c)** OPVA-ZnO-GO (0.5 wt %), **(d)** OPVA-ZnO-GO (1 wt%), and **(e)** OPVA-ZnO-GO (1.5 wt%) membranes.

A weak shoulder observed near 10–12° may correspond to the (001) reflection of GO, indicating partial exfoliation and intercalation within the OPVA matrix [10]. The d-spacing remains constant at 2.48 Å, confirming that GO influences crystallite growth and orientation without altering ZnO's intrinsic lattice parameters. At 1 wt% GO (Fig. 2d), the ZnO peaks, particularly (101) and (002), become sharper and more intense, implying improved crystallite alignment, reduced microstrain, and enhanced templating effects of GO. The crystallite size reaches a maximum of 18.6 nm, while the CI peaks at 0.81, indicating an optimal structural synergy. The GO (001) peak becomes more prominent, confirming its layered integration and structural presence. Mechanistically, this composition achieves an ideal balance among ZnO dispersion, defect passivation, and matrix compatibility; however, at 1.5 wt% GO (Fig. 2e), the ZnO peaks broaden and diminish slightly in intensity, especially the (100) and (102) reflections, indicating increased lattice disorder and potential nanoparticle aggregation. The crystallite size drops to 13.5 nm, and the CI declines to 0.74, reflecting steric hindrance and phase saturation effects. Meanwhile, the GO peak near 10° intensifies, suggesting excessive GO content and partial segregation. These observations align with established saturation thresholds, where surplus GO disrupts ZnO dispersion and compromises matrix uniformity [13]. Quantitative analysis using the Scherrer equation and Bragg's law, based on the (101) peak at $2\theta \approx 36.2^{\circ}$, reveals a non-linear trend in crystallite size and CI across the GO loading series (Table 1). The d-spacing remains constant at 2.48 Å for all ZnO-containing samples, reinforcing that GO modulates crystallite growth and alignment without altering the intrinsic lattice geometry of ZnO.

Structurally, the XRD analysis confirms that GO governs ZnO crystallization through interfacial templating, defect modulation, and steric effects. The optimal structural configuration is achieved at 1 wt% GO, where ZnO crystallinity, peak definition, and matrix integration are maximized. Overall, the XRD results substantiate the hypothesis that GO enhances structural ordering and nanoparticle dispersion in OPVA–ZnO nanocomposites, with 1 wt% GO offering the most favorable balance for optoelectronic, mechanical, and conductive properties.

3.3. Surface morphology via SEM

The SEM micrographs of OPVA–ZnO nanocomposites co-doped with different GO loadings (0.5 wt%, 1 wt%, and 1.5 wt%) demonstrate a gradual transformation in surface morphology and internal structure, reflecting changes in the interfacial architecture and dispersion of ZnO nanoparticles within the oxidized polymer matrix (Fig. 3). Image (a), representing the pristine OPVA membrane, displays a relatively smooth and compact surface with minor undulations, characteristic of semi-

Table 1
Structural Parameters of OPVA–ZnO–GO Nanocomposites and Pristine OPVA Based on the (101) XRD Peak.

Sample	2θ (°)	FWHM (β, rad)	Crystallite Size D (nm)	d-spacing (Å)	Crystallinity Index (CI)
Pristine OPVA	19.5	0.045	3.3	4.55	0.42
OPVA–ZnO	36.2	0.012	12.4	2.48	0.72
OPVA–ZnO–GO (0.5 wt%)	36.2	0.010	14.9	2.48	0.76
OPVA–ZnO–GO (1.0 wt%)	36.2	0.008	18.6	2.48	0.81
OPVA–ZnO–GO (1.5 wt%)	36.2	0.011	13.5	2.48	0.74

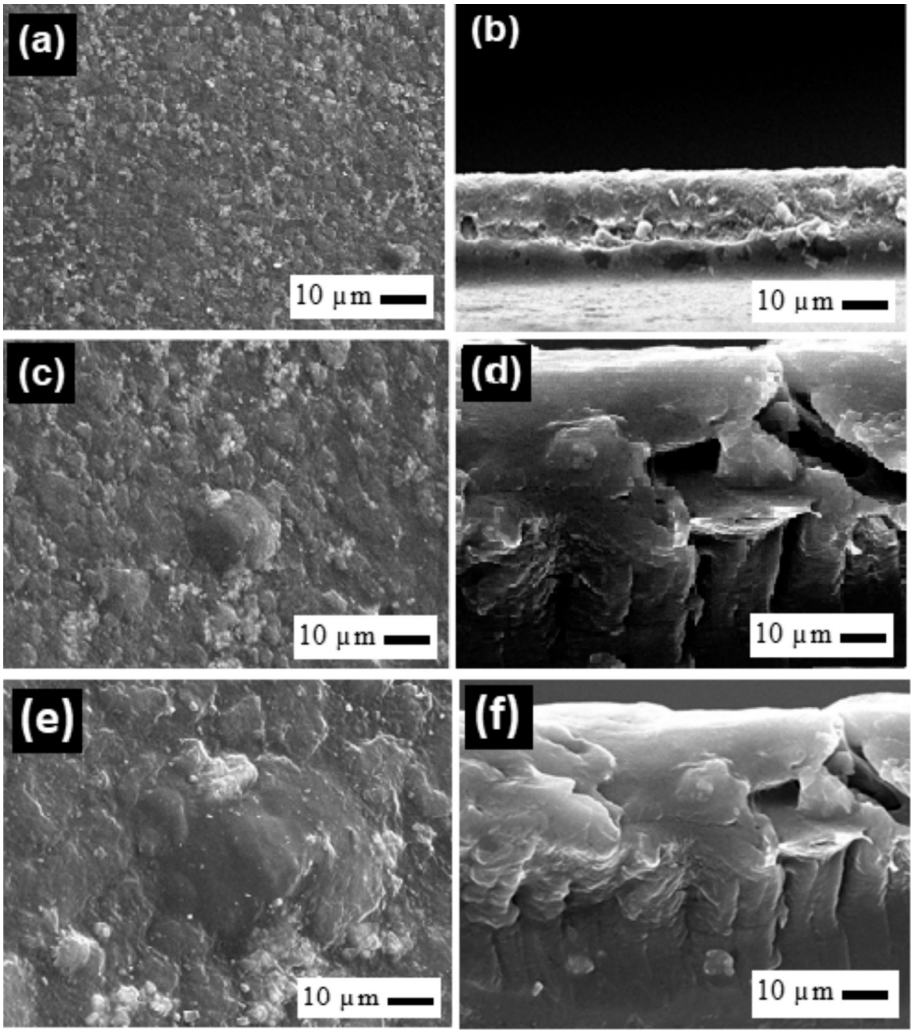

Fig. 3. SEM images of **(a)** pristine OPVA co-doped with 1 wt% ZnO **(c)** with 0.5 wt% and **(e)** 1 wt% and **(b, d, f)** 1.5 wt% GO membranes, along with their corresponding cross-sectional images.

crystalline oxidized PVA. This morphology reflects reduced hydrogen bonding and increased chain packing due to the presence of carbonyl groups [34]. Upon doping with 1 wt% ZnO (image b), the surface shows slight roughening, with visible nanoparticle clusters embedded within the polymer matrix. This observation confirms the *in situ* formation and integration of ZnO nanoparticles, consistent with the morphological trends reported in the original OPVA–ZnO study [4]. The dispersion appears uniform, and no significant agglomeration is observed at this loading, supporting the previously documented enhancement in proton conductivity and optical clarity. The introduction of 0.5 wt% GO (image c) further modifies the surface, producing a more porous and irregular morphology with visible voids and increased roughness. This suggests that GO disrupts polymer packing and introduces additional interfacial complexity. The presence of GO sheets likely enhances ZnO dispersion by anchoring nanoparticles and preventing aggregation, while simultaneously introducing microstructural heterogeneity owing to the layered structure and functional groups of GO [10]. At 1 wt% GO (image d), the surface displays pronounced cracking and delamination, suggesting enhanced interfacial interactions and possible stress accumulation at the ZnO–GO–OPVA interfaces. This morphology reflects a highly integrated ternary network, with GO serving both as a mechanical reinforcer and a dispersion stabilizer, consistent with the optimal spectral synergy observed in FTIR and XRD analyses.

At 1.5 wt% GO (images e and f), surface damage becomes more extensive, exhibiting deep cracks and structural discontinuities. These features suggest that excessive GO oversaturates the matrix, leading to phase separation, steric hindrance, and compromised mechanical integrity. The observed fragmentation and delamination indicate poor stress distribution and reduced matrix cohesion, which may negatively affect flexibility and conductivity. Additional evidence for GO oversaturation at 1.5 wt% is provided by the increased surface hydrophobicity and larger wettability spread values (see Table 1), together with the pronounced surface discontinuities observed in SEM.

Mechanistically, these morphological transitions demonstrate that the influence of GO is dose-dependent: at low to moderate concentrations, it enhances dispersion and interfacial bonding, whereas higher concentrations disrupt matrix uniformity and induce mechanical instability. Overall, SEM analysis validates the hypothesis that GO modulates the microstructure of OPVA–ZnO nanocomposites through interfacial engineering and structural reinforcement, with 1 wt% GO offering the optimal balance between dispersion quality and morphological integrity.

3.4. Surface wettability evolution in OPVA–ZnO–GO nanocomposites

Contact angle measurements of OPVA-based nanocomposites reveal a progressive modulation of surface wettability resulting from nanoparticle incorporation and interfacial chemistry (Table 2).

The pristine OPVA film exhibits a wide range of contact angles (44.3°–83.2°), with an average value of 68.05°, indicative of

Table 2
Contact Angle Variation in OPVA–ZnO–GO nanocomposites.

Sample	Contact Angles (°)	Mean Contact Angle (°)	Spread (Δ)	Surface Interpretation
OPVA	78.3; 83.2; 66.4; 44.3	68.05	38.9	Heterogeneous oxidation; mixed –OH and C═O domains
OPVA–ZnO	110.7; 98.1; 79.0; 102.8	97.65	31.7	ZnO-induced hydrophobicity; reduced surface polarity
OPVA–ZnO–GO 0.5 wt%	71.4; 65.2; 78.6	71.73	13.4	Intermediate wettability; limited GO dispersion
OPVA–ZnO–GO 1.0 wt%	85.8; 54.5; 83.6	74.63	31.3	GO-modulated polarity; partial recovery of hydrophilicity
OPVA–ZnO–GO 1.5 wt%	88.2; 72.5; 95.6	85.43	23.1	GO oversaturation; partial restacking reduces surface polarity and uniformity

heterogeneous surface oxidation. This variability reflects the partial conversion of hydroxyl groups to carbonyl functionalities, resulting in dual-site surface chemistry. The coexistence of hydrophilic –OH and polar C═O groups impart tunable wettability, which is essential for interfacial bonding and functionalization in composite matrices. After ZnO incorporation, the surface becomes markedly more hydrophobic. The OPVA–ZnO sample shows elevated contact angles (mean = 97.65°), consistent with the low surface energy of ZnO and its tendency to mask polar functionalities.

This shift suggests a reduced hydrogen-bonding capacity and diminished surface polarity, most likely due to nanoparticle aggregation or poor interfacial integration. The introduction of GO into the OPVA–ZnO matrix initiates a reversal in wettability. At 0.5 wt% GO, the mean contact angle drops to 71.73°, with a narrow spread (Δ = 13.4°), indicating improved surface uniformity and partial recovery of hydrophilicity. This intermediate response reflects limited GO dispersion, where oxygenated groups begin to reintroduce polarity but do not fully dominate the interface. At 1.0 wt% GO, the system reaches optimal wettability modulation. The mean contact angle further decreases to 74.63°, while the spread remains moderate (Δ = 31.3°), suggesting balanced dispersion and effective surface exposure of GO's functional groups. The presence of –OH, –COOH, and epoxy moieties enhances hydrogen bonding and restores interfacial compatibility, thereby counteracting the hydrophobic influence of ZnO. This composition represents a critical inflexion point at which the surface-modifying role of GO is maximized without triggering morphological instability. Increasing the GO content to 1.5 wt% leads to a rebound in the contact angle (mean = 85.43°), accompanied by a reduced spread (Δ = 23.1°). This behavior is attributed to GO oversaturation, where excess nanosheets restack or phase-separate, thereby limiting the accessibility of hydrophilic sites. Consequently, the surface partially restores its hydrophobic character and uniformity is compromised. The increase in contact angle (Table 2), the larger spread values, and the more pronounced surface discontinuities observed in SEM collectively support the onset of GO oversaturation within the OPVA–ZnO matrix. At this loading, excess GO tends to undergo partial restacking through π–π interactions and insufficient polymer intercalation, reducing the availability of exposed oxygenated groups and thereby decreasing surface polarity. This interpretation is consistent with the decline in crystallinity index observed in XRD and the emergence of microcracks in SEM, both of which point to reduced interfacial compatibility and localized phase segregation at higher GO contents.

Collectively, the results support a mechanistic model in which GO acts as a regulator of surface polarity within OPVA–ZnO composites. While ZnO alone induces hydrophobicity, GO reintroduces hydrophilic functionality, but only within a narrow compositional window. An optimal GO loading of 1 wt% emerges as the most effective condition for achieving balanced wettability, uniform surface chemistry, and enhanced interfacial performance. This insight is significant for the design of nanocomposite membranes, coatings, and optoelectronic platforms where surface energy plays a pivotal role.

3.5. Optical reflectance suppression

The reflectance spectra of OPVA–ZnO nanocomposites co-doped with varying GO ratios (0.5 wt%, 1 wt%, and 1.5 wt%) reveal a distinct and systematic modulation of optical behavior across the UV–Vis range, ascribed to interfacial synergy and nanoscale architecture (Fig. 4).

The pristine OPVA membrane exhibits the highest reflectance, reaching approximately 36% around 400 nm, which is attributed to its semi-crystalline morphology and strong internal scattering from hydroxyl-rich domains. Upon doping with 1 wt% ZnO, the reflectance drops significantly, peaking around 16%, indicating that ZnO nanoparticles disrupt the native packing of OPVA and reduce surface scattering. This observation aligns with the *in situ* ZnO synthesis reported by [4], in which ZnO integration enhances transparency by minimizing bulk scattering and promoting matrix homogenization. Meanwhile, the introduction of GO at 0.5 wt% leads to a further decrease in reflectance, suggesting that GO sheets suppress surface roughness and enhance light absorption through π–π* transitions and defect-mediated scattering. At 1 wt% GO, the reflectance continues to decline, indicating optimal dispersion and interfacial coupling among ZnO, GO, and OPVA. The oxygenated functional groups of GO likely facilitate charge transfer and reduce refractive index mismatch, thereby minimizing Fresnel reflection losses. This trend aligns with prior studies on GO–ZnO–PVA systems, where GO serves as a light-trapping scaffold and enhances dielectric uniformity [10,13].

At 1.5 wt% GO, the reflectance reaches its lowest value across the spectrum, suggesting that excess GO introduces strong absorption and possibly localized plasmonic damping. This may also indicate oversaturation of the matrix, where GO aggregation increases optical density and reduces backscattering. The steep decline in reflectance at shorter wavelengths (300–400 nm) across all GO-doped samples confirms enhanced UV attenuation, which is critical for applications in UV-

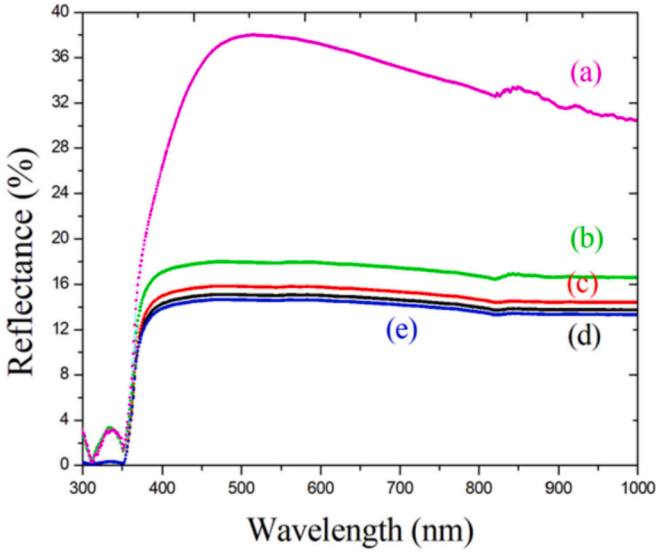

Fig. 4. Reflectance percentage of **(a)** OPVA, **(b)** OPVA-ZnO, **(c)** OPVA-ZnO-GO (0.5 wt%), **(d)** OPVA-ZnO-GO (1 wt%), and **(e)** OPVA-ZnO-GO (1.5 wt %) membranes.

blocking films and transparent coatings. Mechanistically, reflectance suppression is governed by nanoscale interfacial engineering: ZnO contributes to band-edge scattering, GO introduces broadband absorption and defect states, and OPVA provides a tunable dielectric host. The reflectance data validate the hypothesis that GO co-doping modulates the optical response of OPVA–ZnO nanocomposites through the synergistic control of surface morphology, interfacial bonding, and electronic transitions. Among the investigated samples, the 1 wt% GO composite offers the most balanced optical profile, combining low reflectance with structural uniformity, making it particularly suitable for optoelectronic platforms requiring high transparency and UV shielding.

3.6. Transmittance enhancement

The transmittance spectra shown in Fig. 5 complement the reflectance behavior discussed in Fig. 4, offering a coherent picture of how GO co-doping modulates the optical transparency of OPVA–ZnO nanocomposites across the UV–Vis–NIR range.

The pristine OPVA membrane exhibits the lowest transmittance, consistent with its high reflectance and semi-crystalline morphology, which promotes internal scattering and limits light passage. Doping with 1 wt% ZnO markedly increases transmittance, particularly in the visible region, indicating that ZnO nanoparticles disrupt OPVA's dense packing and reduce refractive index mismatch, thereby enhancing light propagation, a trend previously reported by Elleuch et al. [4]. The introduction of 0.5 wt% GO further improves transmittance, suggesting that GO contributes to the suppression of microstructural defects and enhances dielectric homogeneity. At 1 wt% GO, the transmittance curve reaches near-optimal levels, especially within the 400–800 nm range, reflecting a well-balanced composite architecture in which GO sheets are uniformly dispersed and synergistically interact with ZnO and OPVA. This configuration minimizes both surface and bulk scattering, while the π-conjugated domains of GO contribute to broadband absorption and defect passivation [10,13]. Consequently, the composite membrane exhibits high optical clarity and reduced reflectance, making it ideal for applications in transparent electronics and UV shielding. At 1.5 wt% GO, the transmittance reaches its maximum across the spectrum, indicating optimal light passage.

However, this effect may not solely reflect improved transparency; it may also suggest reduced interfacial density or partial phase separation, as excessive GO disrupts matrix cohesion and weakens ZnO–polymer coupling. This interpretation is supported by the concurrent drop in reflectance (Fig. 4), which likely stems from increased GO absorption and reduced backscattering. Mechanistically, the transmittance enhancement is governed by nanoscale dispersion, interfacial bonding, and defect suppression. GO acts as a structural modulator, tuning the optical path and enabling controlled light–matter interactions. Overall, the findings demonstrate that GO co-doping in OPVA–ZnO membranes provides dual advantages, reduced reflectance and enhanced transmittance. The 1 wt% GO composition represents the optimal balance, offering high transparency, minimal scattering, and strong interfacial synergy, key attributes for optoelectronic and photonic applications. Although the reflectance decreases at higher GO loading (1.5 wt%), the corresponding increase in transmittance does not contradict this trend. In thin polymeric films, transmittance is governed not only by absorption but also by surface reflection and scattering. GO incorporation reduces the refractive-index contrast at the air–film interface and introduces nanoscale roughness, both of which suppress Fresnel reflection and act as an anti-reflection mechanism. This reduction in reflectance can therefore increase the forward-scattered light component, leading to an apparent rise in transmittance even when the intrinsic absorbance of the film increases. It is important to note that a decrease in reflectance does not necessarily imply reduced absorbance.

GO possesses strong π–π* and n–π* transitions, and its incorporation is expected to increase absorption, particularly in the UV–visible region. Thus, the observed optical response at 1.5 wt% GO reflects a redistribution of the optical budget ($T + R + A = 1$), where reduced reflectance and enhanced forward scattering outweigh the increase in absorbance. This interpretation is consistent with the darkening of the films at higher GO content and with the known optical behavior of GO-based polymer nanocomposites.

3.7. Photoluminescence

The photoluminescence (PL) spectra of OPVA–ZnO nanocomposites co-doped with varying GO ratios (0.5 wt%, 1 wt%, and 1.5 wt%) under 230 nm excitation reveal critical insights into defect dynamics, energy transfer pathways, and emission tunability, which are key parameters for optoelectronic applications such as UV sensors, light-emitting devices, and transparent photodetectors (Fig. 6).

The OPVA doped with 1 wt% ZnO shows relatively low PL intensity, dominated by a near-band-edge emission around 378 nm and a broader green emission near 534 nm, both characteristic of ZnO's intrinsic

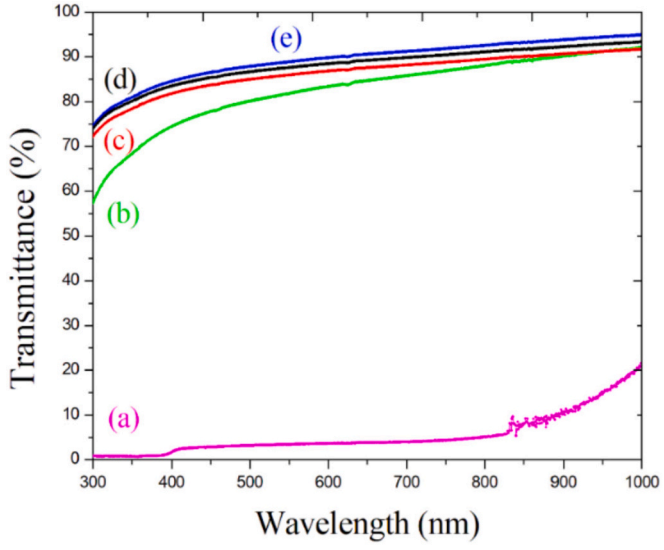

Fig. 5. Transmittance percentage of **(a)** OPVA, **(b)** OPVA-ZnO, **(c)** OPVA-ZnO-GO (0.5 wt%), **(d)** OPVA-ZnO-GO (1 wt%), and **(e)** OPVA-ZnO-GO (1.5 wt %) membranes.

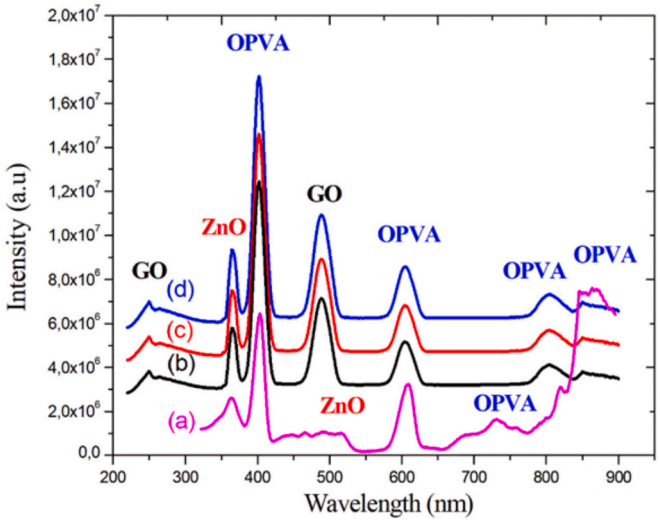

Fig. 6. Photoluminescence spectra of **(a)** OPVA doped ZnO (1 wt%) and OPVA co-doped ZnO (1 wt%) and **(b)** GO (0.5 wt%), **(c)** GO (1.5 wt%), and **(d)** GO (1 wt%) membranes under an excitation wavelength of 230 nm.

excitonic recombination and defect states, such as oxygen vacancies and zinc interstitials [4,16].

The subdued intensity suggests limited radiative recombination efficiency, likely resulting from surface defects and non-radiative pathways within the ZnO lattice. Upon co-doping with 0.5 wt% GO, the PL intensity increases moderately, and the emission profile broadens, indicating that GO begins to interact with ZnO and OPVA at the interface. The oxygenated functional groups of GO may passivate surface defects and facilitate charge transfer, thereby reducing non-radiative losses and enhancing exciton recombination. At 1.5 wt% GO (sample c), the PL intensity reaches its maximum, with sharper and more intense emissions across the visible range. This enhancement is attributed to optimal interfacial synergy, whereby GO acts as a conductive scaffold that stabilizes ZnO dispersion, suppresses defect-mediated recombination, and enables multichannel radiative transitions through π–π* interactions and energy funneling mechanisms [10,13]. Interestingly, the sample with 1 wt% GO shows slightly lower PL intensity than the sample with 1.5 wt% GO, yet displays more well-defined peak positions and narrower bandwidths. This suggests that, while 1.5 wt% GO maximizes emission intensity, 1 wt% GO offers superior spectral purity and reduced background noise, representing an important trade-off for applications requiring wavelength-specific emission, such as tunable light-emitting diodes or narrow-band photodetectors. The presence of OPVA-specific emissions at longer wavelengths (*e.g.*, 621 nm, 742 nm, and 875 nm) across all samples confirms energy transfer between the polymer matrix and ZnO, which is modulated by the presence of GO. These emissions arise from hybridized states and defect-assisted transitions, which are highly desirable for broadband luminescence and near-infrared sensing. Mechanistically, GO enhances PL by passivating ZnO surface defects, facilitating charge separation, and introducing additional radiative centers. Excitation at 230 nm, well above the ZnO bandgap, ensures deep penetration and activates both intrinsic and defect states, rendering the emissions highly sensitive to interfacial chemistry. From an application standpoint, these results underscore the potential of OPVA–ZnO–GO systems in optoelectronics: the tunable PL intensity and spectral distribution can be engineered for UV-blocking coatings, flexible light-emitting films, and hybrid photonic devices. The 1.5 wt% GO sample offers the highest emission output, whereas the 1 wt% GO sample provides spectral refinement, each valuable depending on the target functionality.

3.8. Electrochemical impedance spectroscopy (EIS)

The temperature-dependent proton conductivity profiles presented in Fig. 7 provide compelling evidence that GO co-doping influences ionic transport pathways in OPVA–ZnO nanocomposites.

All samples demonstrate a positive correlation between temperature and conductivity, consistent with a thermally activated conduction mechanism governed by the Arrhenius relation. The reference sample, OPVA doped with 1 wt% ZnO, shows moderate conductivity, reaching ~32 mS/cm at 90 °C. This observation aligns with prior findings [4], where ZnO nanoparticles enhance proton mobility by introducing Lewis acid sites and facilitating hydrogen bonding with the hydroxyl and carbonyl groups of OPVA. Nevertheless, the observed conductivity plateau suggests limited percolation and possible nanoparticle clustering, which restricts long-range proton hopping. Upon co-doping with 0.5 wt% GO, the conductivity improves slightly, indicating that GO contributes to interfacial proton transport.

The oxygenated functional groups of GO (carboxyl, hydroxyl, and epoxy) act as proton donors and acceptors, forming transient hydrogen-bonded networks that support Grotthuss-type proton hopping. Yet, the modest conductivity gain implies that at this loading, GO dispersion is incomplete or its contribution is secondary to the role of ZnO. At 1.5 wt % GO, conductivity increases more substantially, reaching ~48 mS/cm at 90 °C. This enhancement reflects the formation of a hybrid proton-conductive scaffold, in which GO sheets bridge ZnO domains and

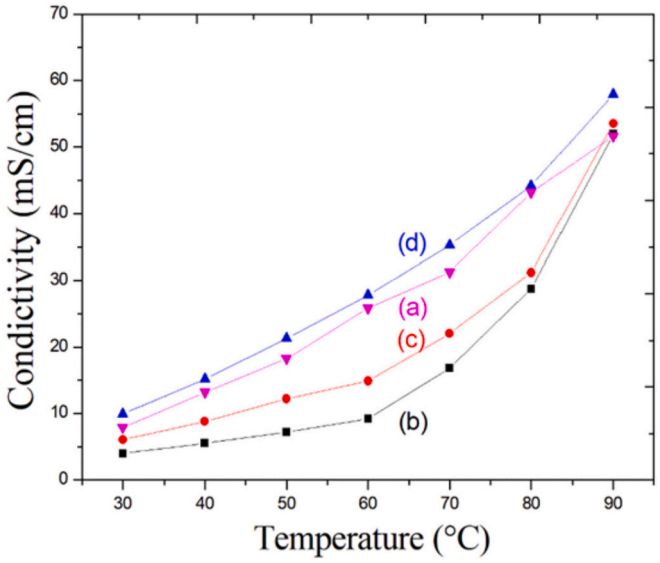

Fig. 7. Temperature-dependent evolution of proton conductivity for **(a)** OPVA doped 1 wt% ZnO and co-doped **(b)** 0.5 wt% GO, **(c)** 1.5 wt% GO, and **(d)** 1 wt % GO membranes.

OPVA chains, creating continuous ionic pathways.

The layered morphology of GO also facilitates water retention and proton solvation, further boosting conductivity under thermal excitation. The highest conductivity is achieved in the 1 wt% GO sample, which peaks at 58.72 mS/cm at 90 °C, suggesting an optimal balance among GO dispersion, ZnO–GO–OPVA interfacial synergy, and matrix hydration. At this ratio, GO is well-integrated, preventing aggregation while maximizing surface area and functional group accessibility. The resulting composite exhibits synergistic benefits from both ZnO's catalytic proton sites and GO's extended hydrogen-bonding network, enabling efficient proton transfer across the membrane. The achieved conductivity matches or [37], positioning OPVA–ZnO–GO membranes as viable candidates for proton exchange membranes in fuel cells, electrochemical sensors, and energy-harvesting devices. Mechanistically, the conductivity enhancement arises from a cooperative effect: ZnO provides localized proton-hopping centers, whereas GO promotes long-range percolation and defect-mediated transport. The temperature-dependent behavior confirms that proton mobility is enhanced through thermal activation of these pathways, with GO playing a critical role in lowering the activation energy and stabilizing the conductive network. Overall, the data validate that GO co-doping improves proton conductivity in OPVA–ZnO systems, with 1 wt% GO offering the most efficient configuration for high-temperature ionic transport. This finding is pivotal for the design of next-generation polymer electrolytes with optimized conductivity, mechanical durability, and optical transparency.

3.9. Mechanical characterization

The mechanical performance of OPVA–ZnO nanocomposites co-doped with different GO ratios (0.5 wt%, 1.0 wt%, and 1.5 wt%) demonstrates a clear and progressive enhancement in structural integrity, stiffness, and ductility, confirming the synergistic reinforcement effect of ZnO and GO within the oxidized polymer matrix (Table 2).

The pristine OPVA membrane exhibits a baseline tensile strength of 13.47 MPa and a Young's modulus of 54.82 MPa, indicating its semi-crystalline structure and moderately developed hydrogen bonding network. Upon doping with 1 wt% ZnO, the tensile strength increases to 16.28 MPa, and the modulus jumps sharply to 280.01 MPa, highlighting the role of ZnO as a rigid nanofiller that interacts with the carbonyl and hydroxyl groups of OPVA to restrict polymer chain mobility and

Table 3
Mechanical Properties of Pure OPVA Membrane, OPVA–ZnO (1% wt) Membrane and OPVA–ZnO Co-Doped with GO (0.5 wt%, 1 wt%, and 1.5 wt%) Membranes.

Sample (wt %)	Tensile strength (MPa)	Young's modulus (MPa)	Stiffness (kN/m)	Elongation at fracture (%)
OPVA	13.47	54.82	11.88	121.91
OPVA-ZnO	16.28	280.01	15.23	128.98
ZnO GO 0.5 wt%	24.85	339.78	18.49	148.86
ZnO GO 1 wt %	25.03	366.54	20.97	154.77
ZnO GO 1.5 wt%	26.09	389.15	18.69	158.04

enhance load transfer [4]. The incorporation of 0.5 wt% GO leads to a substantial enhancement in the mechanical properties: the tensile strength reaches 24.85 MPa, the modulus rises to 339.78 MPa, and the elongation at fracture improves to 148.86%. These findings suggest that GO functions as a stress-distributing scaffold, bridging ZnO domains and reinforcing the polymer matrix through hydrogen bonding and π–π stacking interactions [10]. At 1 wt% GO, the composite achieves near-optimal mechanical synergy, with a tensile strength of 25.03 MPa, modulus of 366.54 MPa, and stiffness of 20.97 kN/m. The elongation at fracture also increases to 154.77%, indicating that GO not only stiffens the matrix but also enhances its ductility by preventing crack propagation and distributing strain energy across the network. Interestingly, at 1.5 wt% GO, the tensile strength and modulus show slight increases (26.09 MPa and 389.15 MPa, respectively), whereas stiffness plateaus and elongation at fracture reaches its highest value (158.04%). These observations indicate that although GO continues to reinforce the matrix, excessive loading may have led to the saturation of interfacial bonding sites, resulting in marginal gains in stiffness and potential onset of aggregation. Nonetheless, the mechanical profile remains superior to that of other compositions, confirming GO's dominant role in enhancing both rigidity and flexibility when optimally dispersed. Notably, the improvements stem from a tri-phase reinforcement strategy: ZnO imparts localized stiffness and interfacial anchoring, GO introduces planar reinforcement and defect bridging, and OPVA offers a flexible yet reactive matrix capable of accommodating both fillers. The observed increase in Young's modulus and tensile strength with GO loading validates the hypothesis that GO acts as a multifunctional mechanical modulator. These results are particularly relevant for applications demanding mechanically robust, flexible, and transparent membranes, such as wearable electronics, flexible sensors, and proton exchange membranes, where structural resilience must be balanced with functional adaptability.

3.10. Mechanistic insights and material design implications

The enhanced performance of OPVA–ZnO–GO nanocomposites originates from the synergistic interplay among molecular functionality, nanoparticle dispersion, and interfacial architecture. Mechanistically, the oxidized backbone of OPVA introduces carbonyl groups that serve as coordination sites for Zn^{2+} ions and as hydrogen-bonding anchors for the oxygenated domains of GO. This chemical reactivity enables *in situ* ZnO nucleation and anchoring while simultaneously facilitating GO integration through electrostatic and π–π interactions. Consequently, a chemically bonded ternary network is formed, supporting defect passivation, charge transfer, and ionic transport. ZnO contributes localized electronic states and catalytic proton sites, whereas GO offers extended percolation pathways and defect-mediated conductivity (Fig. 8).

Meanwhile, the layered morphology of GO enhances mechanical reinforcement and optical modulation by suppressing light scattering and facilitating uniform stress distribution. Spectroscopic analyses confirm that GO alters vibrational dynamics and crystallinity, while PL and conductivity measurements reveal its influence on radiative recombination and proton hopping. Importantly, the optimal GO loading (1 wt%) achieves a balance between interfacial complexity and structural coherence, thereby maximizing performance across all metrics.

From a material design perspective, this system exemplifies how targeted chemical modification, specifically, the oxidation of PVA, can unlock new functionalities into polymer matrices (Fig. 8). The dual role of OPVA as both a reactive host and a flexible scaffold enables precise control over nanoparticle interactions and composite architecture. Furthermore, the *in situ* synthesis approach ensures uniform dispersion and minimizes phase separation, while GO co-doping allows for tunable property enhancement without compromising optical transparency or mechanical flexibility. These insights inform a broader design strategy for multifunctional membranes, involving the combination of chemically active polymers with synergistic nanofillers to achieve simultaneous optical clarity, mechanical resilience, and ionic conductivity. The OPVA–ZnO–GO platform thus offers a scalable and adaptable framework for next-generation applications in flexible electronics, transparent

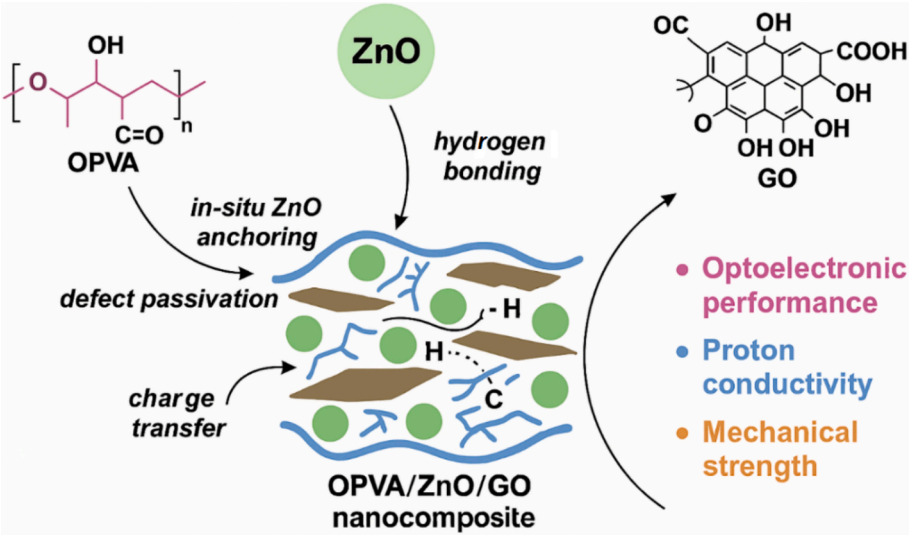

Fig. 8. Interfacial synergy and Functional enhancement in OPVA–ZnO–GO nanocomposites: Mechanistic insights into multifunctional performance.

coatings, UV-blocking films, and energy conversion devices.

4. Conclusion

This study indicates that the increased performance of OPVA-ZnO-GO nanocomposites is due to the synergistic interaction between ZnO and GO, which results in multifunctional materials with tunable optoelectronic, mechanical, and proton-conductive capabilities. Unlike standard PVA, OPVA's carbonyl-rich backbone allows for greater interfacial coordination with ZnO and GO, resulting in uniform nanoparticle dispersion, increased hydrogen bonding, and defect passivation. Spectroscopic investigations (FTIR, XRD, and PL) indicated the creation of a chemically integrated ternary network, while SEM showed increased morphological integrity and reduced aggregation at optimal GO loadings. Optical measurements revealed a simultaneous drop in reflectance and rise in transmittance, especially at 1 wt% GO, indicating improved transparency and UV-blocking capabilities. The PL spectra indicated variable emission patterns, with 1.5 wt% GO improving intensity and 1 wt% GO enhancing spectrum purity, both beneficial for light-emitting and sensing applications. The 1 wt% GO sample had a maximal proton conductivity of 58.72 mS/cm, indicating its ability to construct continuous ionic channels and decrease activation energy. Mechanical testing indicated that GO co-doping increased tensile strength, modulus, and elongation, with OPVA-ZnO-GO membranes surpassing PVA-based equivalents in all parameters. Overall, these findings point to OPVA-ZnO-GO nanocomposites as interesting options for flexible optoelectronic devices, transparent coatings, proton exchange membranes, and wearable technology. The combination of OPVA's reactive matrix, ZnO's functional nanostructure, and GO's interfacial adaptability establishes a novel approach in polymer nanocomposite synthesis.

CRediT authorship contribution statement

Ridha Elleuch: Writing – review & editing, Writing – original draft, Methodology, Formal analysis, Data curation. **Khaled Charradi:** Writing – review & editing, Writing – original draft, Validation, Methodology, Investigation, Conceptualization. **Abdullah Y.A. Alzahrani:** Validation, Supervision, Resources, Investigation, Conceptualization. **Soad Z. Alsheheri:** Writing – original draft, Validation, Investigation, Formal analysis. **Akram Alhussein:** Writing – original draft, Visualization, Validation, Resources, Funding acquisition, Formal analysis. **Youssef O. Al-Ghamdi:** Writing – original draft, Validation, Resources, Methodology, Investigation, Conceptualization. **Sherif M.A.S. Keshk:** Writing – review & editing, Writing – original draft, Validation, Methodology, Investigation, Conceptualization.

Declaration of competing interest

The authors declare that they have no known competing financial interests or personal relationships that could have influenced the work reported in this paper.

Acknowledgment

The authors extend their appreciation to the Deanship of Research and Graduate Studies at King Khalid University for funding this work through a Large Research Project under grant number RGP 2/363/46.

Declaration of competing interest

The authors declare that they have no known competing financial interests or personal relationships that could have appeared to influence the work reported in this paper.

Data availability

No data was used for the research described in the article.

References

[1] K. Charradi, Z. Ahmed, M. Chemek, Y.O. Al-Ghamdi, R. Chtourou, S.M.A.S. Keshk, Highly conducting solid electrolyte films based on divalent cations (Zn, Fe, Ni)/oxidized PVA composites, J. Non-Cryst. Solids 588 (2022) 121609, https://doi.org/10.1016/j.jnoncrysol.2022.121609.
[2] K. Charradi, M. Chemek, B. Slimi, A.M. Ramadan, A.Y.A. Alzahrani, R. Chtourou, S. M.A.S. Keshk, Proton conductivity and optical performance studies on polyvalent metals/oxidized polyvinyl alcohol composites, J. Polym. Environ. 31 (2023) 3167–3181, https://doi.org/10.1007/s10924-023-05432-5.
[3] W.A. Bawazir, Q.A. Alsulami, S.M.A.S. Keshk, Novel approach to ameliorate proton conductivity of poly(vinyl alcohol) via crosslinking with poly(vinyl pyrrolidone), J. Appl. Polym. Sci. 140 (2023) e53812, https://doi.org/10.1002/app.53812.
[4] R. Elleuch, et al., In-situ synthesis of ZnO nanoparticles in oxidized polyvinyl alcohol nanocomposites for tunable optoelectronic and proton conductive performance, Mater. Sci. Eng. B 321 (2025) 118538, https://doi.org/10.1016/j.mseb.2025.118538.
[5] A. Siai, A.Y.A. Al-Zahrani, R. Chtourou, S.M.A.S. Keshk, Enhanced lithium-ion transport in oxidized polyvinyl alcohol/$La_{0.56}Li_{0.33}TiO_3$ hybrid electrolytes for solid-state batteries, J. Phys. Chem. Solids 208 (2026) 113048, https://doi.org/10.1016/j.jpcs.2026.113048.
[6] A. Alkabsh, Synthesis, structural, optical and photoluminescence properties of hybrid PVA/ZnO nanocomposite membrane, J. Opt. 53 (2024) 253–265, https://doi.org/10.1007/s12596-024-00653-2.
[7] A.R. Kachere, P.M. Kakade, A.R. Kanwade, P. Dani, N.T. Mandlik, S.R. Rondiya, N. Y. Dzade, S.R. Jadkar, S.V. Bhosale, Zinc oxide–graphene oxide nanocomposites: synthesis, characterization and their optical properties, ES Mater. Manuf. 16 (2022) 19–29, https://doi.org/10.30919/esmm5f516.
[8] Z. Landolsi, K. Charradi, W. Mabrouk, A.M. Ramadan, Q.A. Alsulami, D. Nunes, S. M.A.S. Keshk, High-performance OPVA/CMC hybrid biopolymer electrolyte with enhanced proton conductivity for SBPE applications, Emerg. Mater. 78 (2025) 01146, https://doi.org/10.1007/s42247-025-01146-8.
[9] M. Muradov, E. Huseynov, M. Conradi, M. Malok, T. Sever, M.B. Baghirov, Effects of gamma radiation on the properties of GO/PVA/AgNW nanocomposites, RSC Adv. 15 (2025) 13574–13584, https://doi.org/10.1039/d5ra01344e.
[10] S. Padinhattayil, K.S. Rai, PVA/GO-ZnO hybrid nanocomposites: synthesis, analysis and applications, Indian, J. Sci. Technol. 14 (2021) 1982–1992, https://doi.org/10.17485/IJST/v14i23.236.
[11] S. Baachaoui, W. Mabrouk, K. Charradi, B. Slimi, A.M. Ramadan, R.M.I. Elsamra, A. Alhussein, S.M.A.S. Keshk, N. Raouafi, Laser-induced porous graphene electrodes from polyketimine membranes for paracetamol sensing, R. Soc. Open Sci. 10 (2023) 230294, https://doi.org/10.1098/rsos.230294.
[12] M. Buldu-Akturk, M. Toufani, A. Tufani, E. Erdem, ZnO and reduced graphene oxide electrodes for all-in-one supercapacitor devices, Nanoscale 14 (2022) 3269–3278, https://doi.org/10.1039/D2NR00018K.
[13] M. Morget, N. Prasad, M.M. Sivalingam, D. Sastikumar, B. Karthikeyan, Optical and phonon properties of ZnO–GO–PVA nanocomposite films for UV sensing, J. Mater. Sci. Mater. Electron. 29 (2018) 365–373, https://doi.org/10.1007/s10854-017-7925-z.
[14] S. Asadpour, A. Gholami, M. Shabani, A review on zinc oxide/poly(vinyl alcohol) nanocomposites: synthesis, characterization and applications, J. Clean. Prod. 362 (2022) 132297, https://doi.org/10.1016/j.jclepro.2022.132297.
[15] M. Ben Hadj Said, K. Charradi, Z. Ahmed, H. Cachet, C. Debiemme-Chouvy, Q. A. Alsulami, S. Boufi, S.M.A.S. Keshk, R. Chtourou, Synthesis and characterization of cellulose hydrogel/graphene oxide/polyaniline composite for high-performing supercapacitors, Int. J. Energy Res. 46 (2022) 13844–13854, https://doi.org/10.1002/er.7654.
[16] X. Fang, T. Zhai, U.K. Gautam, L. Li, L. Wu, Y. Bando, D. Golberg, ZnS nanostructures: from synthesis to applications, Prog. Mater. Sci. 56 (2011) 175–287, https://doi.org/10.1016/j.pmatsci.2010.10.001.
[17] M. Cobos, M.J. Fernández, M.D. Fernández, Graphene based poly(vinyl alcohol) nanocomposites prepared by in situ green reduction of graphene oxide by ascorbic acid: influence of graphene content and glycerol plasticizer on properties, Nanomaterials 8 (2018) 1013, https://doi.org/10.3390/nano8121013.
[18] A. Haouas, A. Boussaid, M. Salem, A. Almohammedi, H. Ghannam, Interfacial treatment insights of promising ternary cu-doped ZnO–GO thin films for improved silicon surface passivation, J. Mater. Sci. Mater. Electron. 36 (2025) 364, https://doi.org/10.1007/s10854-025-14434-6.
[19] B.G. Suma, Y. Sangappa, ZnO/GO nanocomposites: synthesis, structural, optical and electrical properties for optoelectronic applications, Mater. Today Proc. 84 (2024) 1464–1470, https://doi.org/10.1016/j.matpr.2024.05.146.
[20] A. Asture, V. Rawat, C. Srivastava, D. Vaya, Investigation of properties and applications of ZnO polymer nanocomposites, Polym. Bull. 80 (2022) 3507–3545, https://doi.org/10.1007/s00289-022-04243-w.
[21] Y. Zhu, J. An, R.S. Ruoff, Graphene-based ultracapacitors: enhanced performance via ZnO–GO hybridization, Nano Energy 98 (2025) 107345, https://doi.org/10.1016/j.nanoen.2025.107345.
[22] M. Saranya, R. Ramachandran, F. Wang, Graphene–zinc oxide (G–ZnO) nanocomposite for electrochemical supercapacitor applications, J. Sci. Adv. Mater. Devices 1 (2016) 454–460, https://doi.org/10.1016/j.jsamd.2016.10.005.

[23] P. Rauwel, M. Salumaa, A. Aasna, A. Galeckas, E. Rauwel, A review of the synthesis and photoluminescence properties of hybrid ZnO and carbon nanomaterials, J. Nanomater. 2016 (2016) 5320625, https://doi.org/10.1155/2016/5320625.
[24] S.Y. Sawant, M.H. Cho, Facile electrochemical assisted synthesis of ZnO/graphene nanosheets with enhanced photocatalytic activity, RSC Adv. 5 (2015) 96189–96197, https://doi.org/10.1039/C5RA22372E.
[25] A.T. Smith, A.M. LaChance, S. Zeng, B. Liu, L. Sun, Synthesis, properties, and applications of graphene oxide/reduced graphene oxide and their nanocomposites, Nano, Mater. Sci. 1 (2019) 31–47, https://doi.org/10.1016/j.nanoms.2019.02.004.
[26] A. Razaq, F. Bibi, X. Zheng, R. Papadakis, S.H.M. Jafri, H. Li, Review on graphene-, graphene oxide-, reduced graphene oxide-based flexible composites: from fabrication to applications, Mater 15 (2022) 1012, https://doi.org/10.3390/ma15031012.
[27] G. Prasad, S. Tamang, S. Jha, N.K. Bhattacharyya, J. Biswas, A theoretical insight into graphene-based materials: a DFT study, Results Surf. Interfaces 18 (2025) 100463, https://doi.org/10.1016/j.rsurfi.2025.100463.
[28] S. Ruan, Y. Zhao, R. Chen, et al., Effect of zinc oxide/graphene oxide nanocomposites on the cytotoxicity, antibacterial and mechanical properties of polymethyl methacrylate, BMC Oral Health 24 (2024) 1013, https://doi.org/10.1186/s12903-024-04754-0.
[29] Q.A. Alsulami, K. Charradi, F.M. Alshareef, S.M.A.S. Keshk, Fabrication of transparent, dopant-free OPVA–GO nanocomposites with tunable proton conductivity and optical transparency for photonic and energy applications, Mater. Renew. Sustain. Energy (2026), https://doi.org/10.1007/s40243-026-00353-x.
[30] Y. Zhang, Z. Shi, X. Cui, S. Zhuang, B. Wu, X. Chu, X. Dong, B. Zhang, G. Du, Enhanced photoluminescence and defect modulation in ZnO/graphene oxide nanocomposites under UV excitation, Mater. Chem. Front. 1 (2017) 1413–1421, https://doi.org/10.1039/C7QM00058H.
[31] F. Omri, W. Selmi, M. Saidani, H.E. Ali, J.L. Lazzari, M. Bendahan, S.M.A.S. Keshk, W. Dimassi, Multifunctional nanocomposites for optical and antimicrobial applications, Adv. Opt. Mater. (2025) 2500980, https://doi.org/10.1002/adom.202500980.
[32] H. Ozlu, D. Yildiz, M.M. Demir, Graphene/ZnO hybrid nanocomposites electrode material for high-performance supercapacitor application, J. Electron. Mater. 54 (2024) 1218–1227, https://doi.org/10.1007/s11664-024-11650-4.
[33] V. Pasindu, P. Yapa, S. Dabare, I. Munaweera, Multifunctional transition metal oxide/graphene oxide nanocomposites for catalytic dye degradation, renewable energy, and energy storage applications, RSC Adv. 15 (2025) 33162–33186, https://doi.org/10.1039/D5RA04806K.
[34] K. Charradi, M. Daoudi, M. Chemek, Z. Ahmed, A.Y.A. Alzahrani, A. Siai, R. Chtourou, Synthesis, characterization and optical properties of oxidized polyvinyl alcohol, Chem. Select 7 (2022) e202103273, https://doi.org/10.1002/slct.202103273.
[35] D.C. Marcano, D.V. Kosynkin, J.M. Berlin, A. Sinitskii, Z. Sun, A. Slesarev, L. B. Alemany, W. Lu, J.M. Tour, Improved synthesis of graphene oxide, ACS Nano 4 (2010) 4806–4814, https://doi.org/10.1021/nn1006368.
[36] S. Dacrory, Development of mesoporous foam based on dicarboxylic cellulose and graphene oxide for potential oil/water separation, Polym. Bull. 79 (2022) 9563–9574, https://doi.org/10.1007/s00289-021-03963-9.
[37] L. Liu, W. Chen, Y. Li, An overview of the proton conductivity of Nafion membranes through a statistical analysis, J. Membr. Sci. 504 (2016) 1–9, https://doi.org/10.1016/j.memsci.2015.12.065.